Supplementary Information (SI) for Journal of Materials Chemistry A.
This journal is © The Royal Society of Chemistry 2024

Effect of molecular size on the electrocatalytic activity of M-N_4-C catalysts for ORR, OER, and HER

Liang Xie[a], Wei Zhou[a*], Zhibin Qu[a], Xiaoxiao Meng[a], Yuming Huang[a], Xuewei Zhang[a], Chaowei Yang[a], Junfeng Li[a], Jingyu Li [a], Fei Sun[a], Jihui Gao[a], Guangbo Zhao[a].

a School of Energy Science and Engineering, Harbin Institute of Technology, Harbin, Heilongjiang, 150001 P. R. China

* Corresponding author: Wei Zhou

E-mail address: hitzhouw@hit.edu.cn

Calculation method

S1. Computational software and methods

All density functional theory (DFT) calculations were performed using the Gaussian 09 code[1]. Geometry optimization and frequency analysis were conducted at the wb97xd/def2svp level of theory[2,3]. The SMD implicit solvation model was employed to simulate the solvent environment[4]. The Gibbs free energy of the catalysts and adsorption configurations was calculated using the following formula: G = G_vac + △G_sol, where G_vac is the free energy under vacuum conditions, and △G_sol represents the effect of the solvent environment on the free energy[5]. It should be noted that although hydrogen bonding between water molecules in explicit solvation models can influence the reaction process[6], here we focus on the implicit solvation model for describing nC@MN_4, which is sufficient for the purposes of this study. Since this work mainly focuses on the impact of size on the true activity origin of MN_4, the complexities of solvent-induced effects due to size variations are not considered within the scope of this study.

S2. Structural analysis and calculation

The formation energy (E_f) in this work was calculated using the following formula:

$$E_f = E_{M-N_4-C} - E_{N_4-C} - E_M \quad (1)$$

where E_{M-N_4-C}, E_{N_4-C}, and E_M represent the electronic energy of the carbon-based single-atom M-N_4-C, the N_4-C structure without the metal center, and the metal center atom, respectively.

In this study, the following electronic and geometric structures were described and analyzed: the average charge of nC@MN_4 centered on the metal atom, the charge and spin population at the metal center, the d-band center of the metal atom, the fundamental gap, the average M-N bond length, and the size.

Atomic charges, spin populations, and the metal atom d-band center were obtained using the Multiwfn code[7]. The charge analysis was carried out using the Atomic Dipole Moment Corrected Hirshfeld (ADCH) method[8]. The average charge of nC@MN_4 centered on the metal atom was calculated using the formula:

$$Charge_{average} = \frac{\sum Charge_i}{n} \quad (2)$$

where $\sum Charge_i$ is the sum of the atomic charges in layer i, and n is the total number of atoms in that layer. Spin population, defined as the alpha population minus the beta population, was obtained using the Mulliken method. The d-band center of the metal atom was calculated using the following formula[9,10]:

$$\text{d band center} = E_{c,M} - E_F \quad (3)$$

Here, $E_{c,M}$ refers to the energy of the d-band position center of the metal M, calculated by the formula:

(4)

$$E_{c,M} = \frac{\int_{low}^{high} E \times PDOS_F(E)dE}{\int_{low}^{high} PDOS_F(E)dE}$$

E_F refers to the Fermi energy level, and for the isolated system model used in this study, we adopt the energy level of the Highest Occupied Molecular Orbital (HOMO).

The Fundamental Gap (E_g) was proposed to describe the electron supply capacity of the nC@MN_4 system. It is calculated by subtracting the Vertical Electron Affinity (VEA) from the Vertical Ionization Potential (VIP)[11,12]:

$$E_g = VIP - VEA = (E_{(N-1)} - E_{(N)}) + (E_{(N+1)} - E_{(N)}) = E_{(N-1)} + E_{(N+1)} - 2* E_{(N)} \quad (5)$$

where $E_{(N-1)}$, $E_{(N+1)}$, and $E_{(N)}$ represent the electronic energies of the Sub@MN_4 model with N-1, N+1, and N electrons, respectively.

For geometric structure parameters, the atomic distances were measured directly. The average M-N bond length was calculated using the formula:

$$L_{M-N} = \frac{\sum l_i}{4} \quad (6)$$

where l_i represents the length of the i-th M-N bond. The size was determined by measuring the distance between the two farthest hydrogen atoms along the horizontal axis in the structure.

S3. Gibbs free energy calculation

S3.1 Calculation of Gibbs free energy for the ORR/OER process

ORR and OER are two reversible reactions, as shown in the following equations. Under acidic conditions, the reaction from left to right represents ORR, which produces H_2O, while the reaction from right to left represents OER, which generates O_2.

$$4H^+ + O_2 + 4e^- \leftrightarrow 2H_2O \quad (7)$$

The entire ORR process consists of four steps, each of which involves proton-coupled electron transfer reactions, as previously reported[13] :

$$*+O_2+ H^++e^-\rightarrow *OOH \quad (8)$$

$$*OOH+ H^++e^-\rightarrow *O+H_2O \quad (9)$$

$$*O+ H^++e^-\rightarrow *OH \quad (10)$$

$$*OH+ H^++e^-\rightarrow *+H_2O \quad (11)$$

Here, * represents the active site of the catalyst, *OOH, *O, and *OH are the corresponding

adsorbed intermediates. To calculate the Gibbs free energy change for each individual step, the experimentally measured reaction energy of $2H_2O \rightarrow O_2 + 2H_2$ (4.92 eV) is used to calculate the free energy of O_2 gas. The CHE model is employed to equate the chemical potential of gaseous hydrogen under standard conditions to the chemical potential of the proton-electron pair . The influence of electrode potential U on the electron e is expressed through -eU, and the effect of pH is calculated using kbTln10 × pH. The calculation of the Gibbs free energy change for each step is as follows[13]:

$$\Delta G_3 = \Delta G_{*OOH} - 4.92\ eV + eU + k_bTln10 \times pH \quad (12)$$

$$\Delta G_4 = \Delta G_{*O} - \Delta G_{*OOH} + eU + k_bTln10 \times pH \quad (13)$$

$$\Delta G_5 = \Delta G_{*OH} - \Delta G_{*O} + eU + k_bTln10 \times pH \quad (14)$$

$$\Delta G_6 = -\Delta G_{*OH} + eU + k_bTln10 \times pH \quad (15)$$

The values of ΔG_{*OOH}, ΔG_{*O}, ΔG_{*OH} are calculated through the following reactions ($2H_2O+*\rightarrow *OOH+3/2H_2$, $H_2O+*\rightarrow *O+H_2$, $H_2O+*\rightarrow *OH+1/2H_2$):

$$\Delta G_{*OOH} = G_{*OOH} - G_* - (2G_{H2O} - 3/2G_{H2}) \quad (16)$$

$$\Delta G_{*O} = G_{*O} - G_* - (G_{H2O} - G_{H2}) \quad (17)$$

$$\Delta G_{*OH} = G_{*OH} - G_* - (G_{H2O} - 1/2G_{H2}) \quad (18)$$

Among these four steps, the rate-determining step is defined as the one with the largest Gibbs free energy change. Therefore, the overpotential of ORR can be calculated using the following equation:

$$\eta_{ORR} = \max\{\Delta G_{3\text{-}e}, \Delta G_{4\text{-}e}, \Delta G_{5\text{-}e}, \Delta G_{6\text{-}e}\}/e + 1.23 \quad (19)$$

As OER is the reversible reaction of ORR, the overpotential can be calculated using the following equation:

$$\eta_{OER} = -\min\{\Delta G_{3\text{-}e}, \Delta G_{4\text{-}e}, \Delta G_{5\text{-}e}, \Delta G_{6\text{-}e}\}/e - 1.23 \quad (20)$$

It is worth noting that HER, OER, and ORR are reactions that occur at different electrode potentials, and thus, they do not compete selectively with each other. Specifically, in the water splitting system, when a positive potential exceeding 1.23V is applied, the OER reaction takes place at the anode, whereas when a negative potential below 0V is applied, the HER reaction occurs at the cathode. In the case of metal-air batteries, ORR will occur when the applied positive potential is between 0 to 1.23V, while OER will occur when the applied positive potential exceeds 1.23V.

S3.2 Calculation of Gibbs free energy for the HER process

The HER reaction energy can be described by the following equation:

$$2H^+ + 2e^- \rightarrow H_2 \quad (21)$$

This process is divided into the following two steps:

$$*+ H^{+}+e^{-}\rightarrow *H \quad (22)$$

$$*H+H^{+}+e^{-}\rightarrow *+ H_2 \quad (23)$$

In the equations provided, * represents the active site of the catalyst, and *H is the adsorbed intermediate of the HER process. The CHE model is used to equate the chemical potential of gaseous hydrogen under standard conditions to the chemical potential of the proton-electron pair . The influence of electrode potential U on the electron e is expressed through -eU, and the (24) pH is calculated using kbTln10 × pH. The calculation of the Gibbs free energy change for each step is as follows[13]:

$$\Delta G_{16} = \Delta G_{*H} + eU + k_b T\ln 10 \times pH$$

$$\Delta G_{17} = -\Delta G_{*H} + eU + k_b T\ln 10 \times pH \quad (25)$$

Where $\Delta G_{*H} = G_{*H} - G_{*} - 1/2G_{H2}$.

The overpotential of the entire reaction is:

$$H_{HER} = \max\{\Delta G_{16}, \Delta G_{17}\}/e \quad (26)$$

Table S1 Spin configurations used for the adsorption structures in nC@FeN_4 reactions.

	10C@FeN_4	36C@FeN_4	74C@FeN_4	124C@FeN_4	186C@FeN_4
*	3	3	3	5	3
*OOH	2	2	2	2	2
*O	3	3	3	3	3
*OH	2	2	4	2	4
*H	2	2	2	4	2

Table S2 Spin configurations used for the adsorption structures in nC@CoN_4 reactions.

	10C@CoN_4	36C@CoN_4	74C@CoN_4	124C@CoN_4	186C@CoN_4
*	2	4	2	4	2
*OOH	1	1	1	1	1
*O	2	2	2	2	2
*OH	1	1	1	1	1
*H	1	1	1	1	1

Table S3 Spin configurations used for the adsorption structures in nC@NiN_4 reactions.

	10C@NiN_4	36C@NiN_4	74C@NiN_4	124C@NiN_4	186C@NiN_4
*	1	1	1	1	1
*OOH	2	2	2	2	2
*O	3	1	3	3	3
*OH	2	2	2	2	2
*H	2	2	2	2	2

Table S4 Spin configurations used for the adsorption structures in nC@CuN_4 reactions.

	10C@CuN_4	36C@CuN_4	74C@CuN_4	124C@CuN_4	186C@CuN_4
*	2	2	2	2	2
*OOH	1	1	3	1	1
*O	2	2	4	4	4
*OH	3	1	3	3	1
*H	1	1	1	1	1

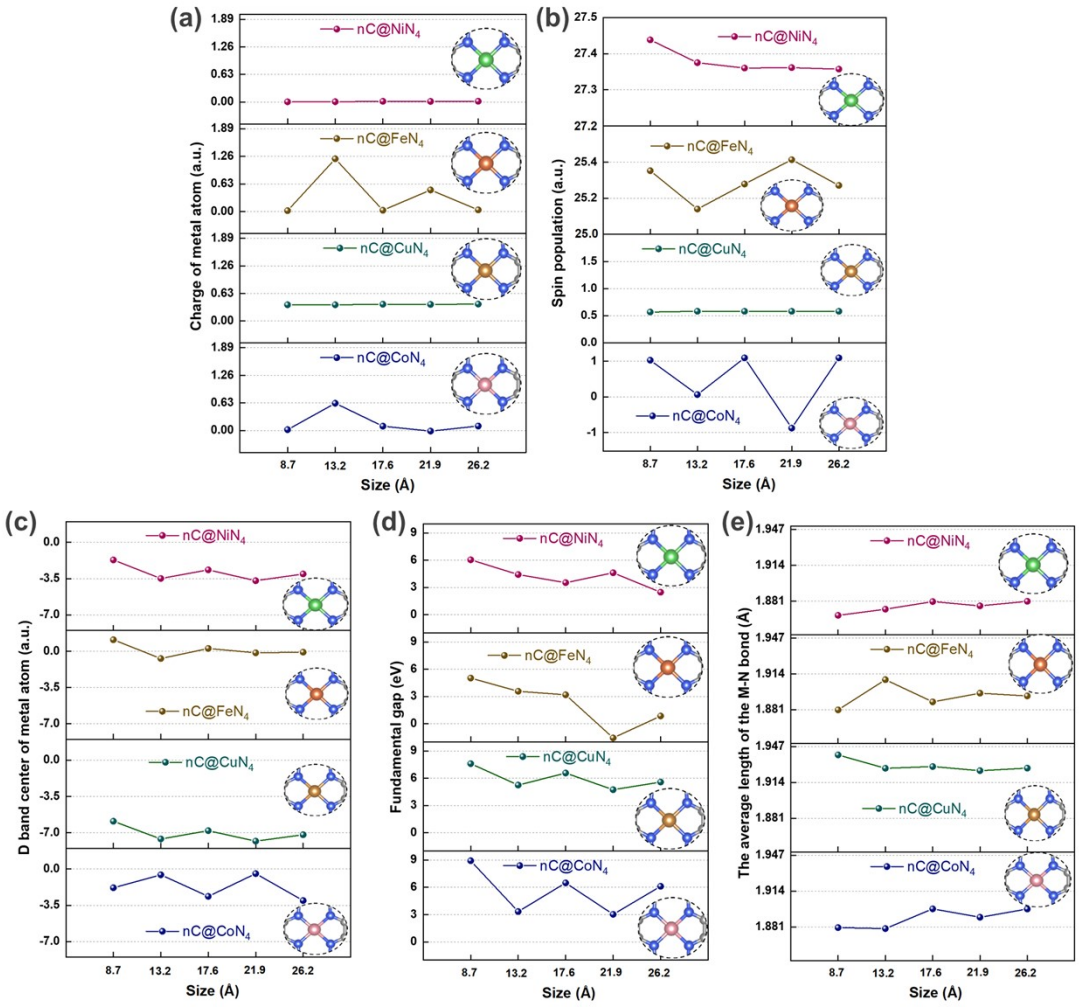

Figure S1. Size-dependent variations in nC@MN_4 (M = Ni, Fe, Cu, Co): (a) Metal center charge; (b) Spin population; (c) Metal atom d-band center; (d) Fundamental gap; (e) Average M-N bond length.

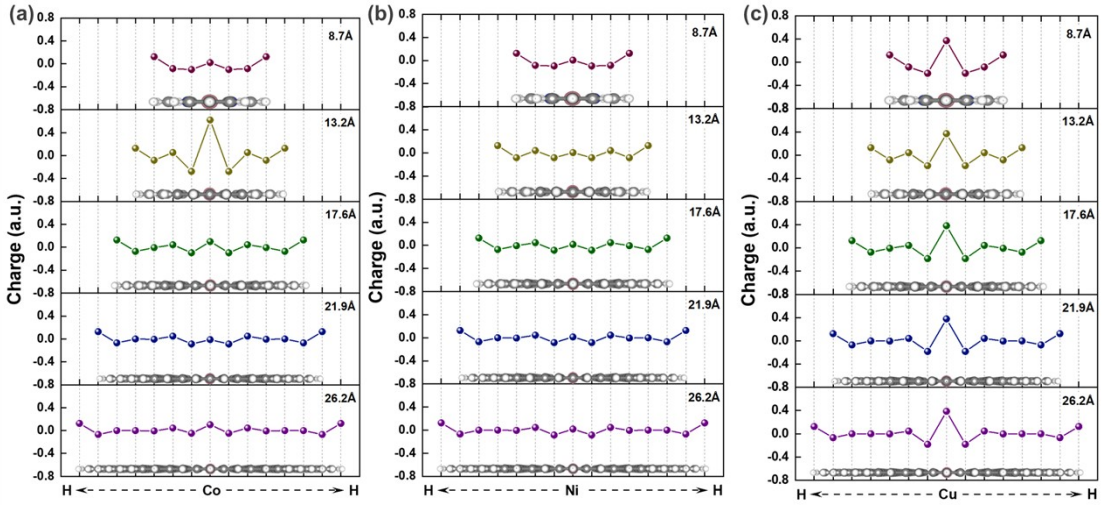

Figure S2. Average charge distribution centered on the metal atom in (a) nC@CoN_4, (b) nC@NiN_4, (c) nC@CuN_4.

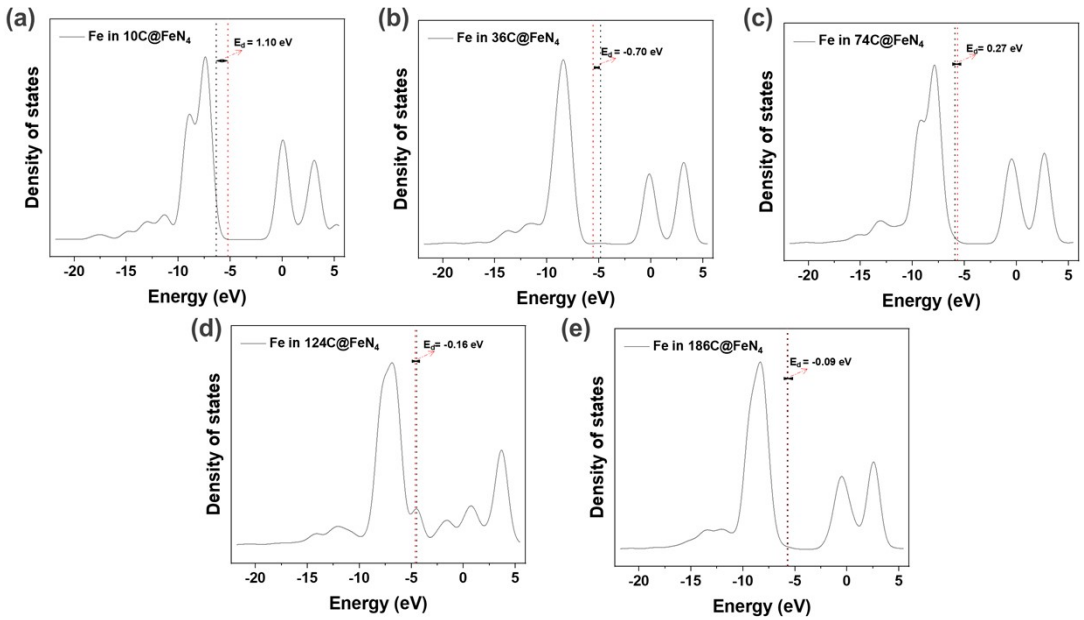

Figure S3. d-band center of Fe in nC@FeN_4. (a) 10C@FeN_4; (b) 36C@FeN_4; (c) 74C@FeN_4; (d) 124C@FeN_4; (e) 186C@FeN_4.

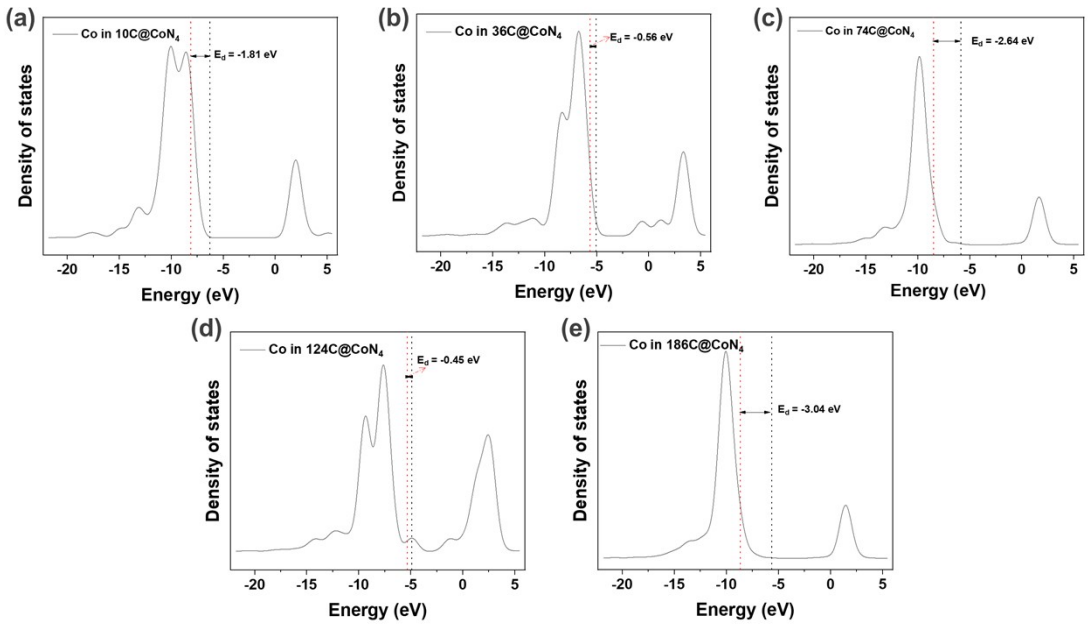

Figure S4. d-band center of Co in nC@CoN_4. (a) 10C@CoN_4; (b) 36C@CoN_4; (c) 74C@CoN_4; (d) 124C@CoN_4; (e) 186C@CoN_4.

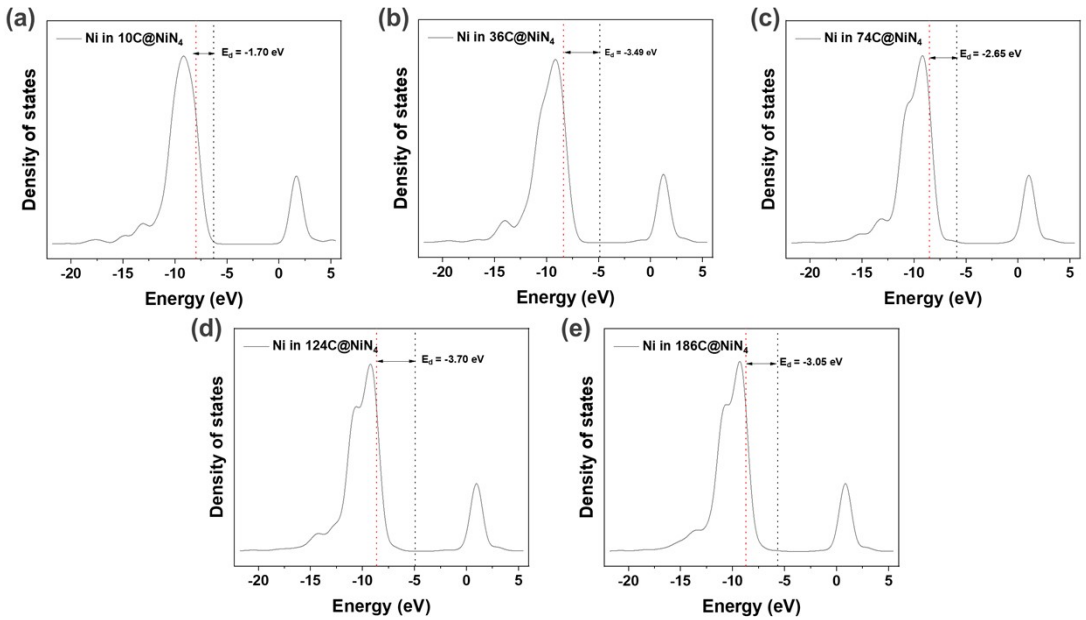

Figure S5. d-band center of Ni in nC@NiN_4. (a) 10C@NiN_4; (b) 36C@NiN_4; (c) 74C@NiN_4; (d) 124C@NiN_4; (e) 186C@NiN_4.

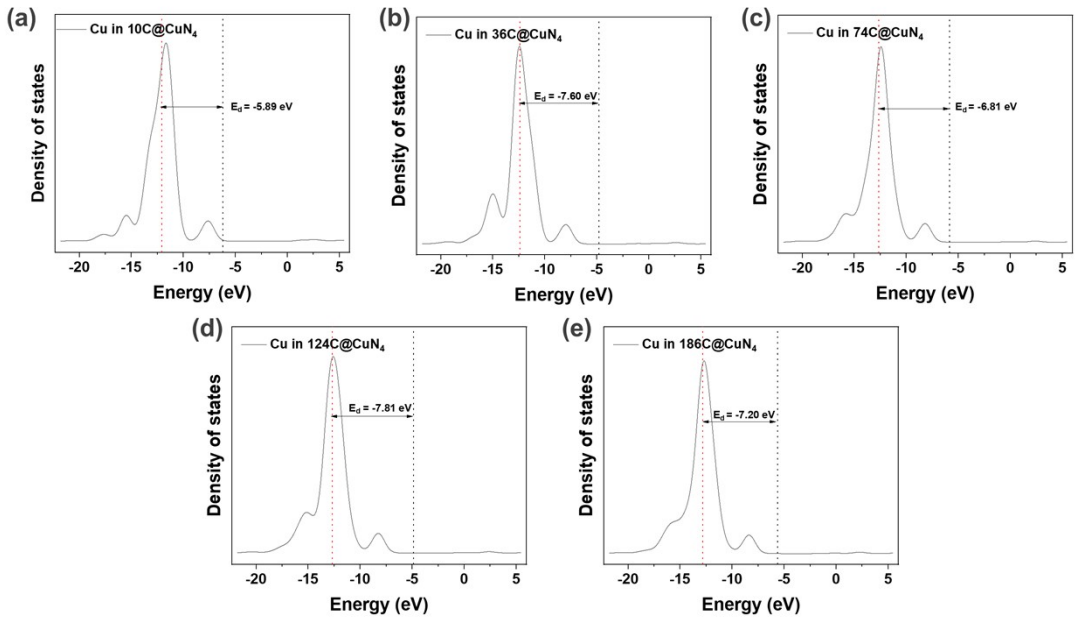

Figure S6. d-band center of Cu in nC@CuN_4. (a) 10C@CuN_4; (b) 36C@CuN_4; (c) 74C@CuN_4; (d) 124C@CuN_4; (e) 186C@CuN_4.

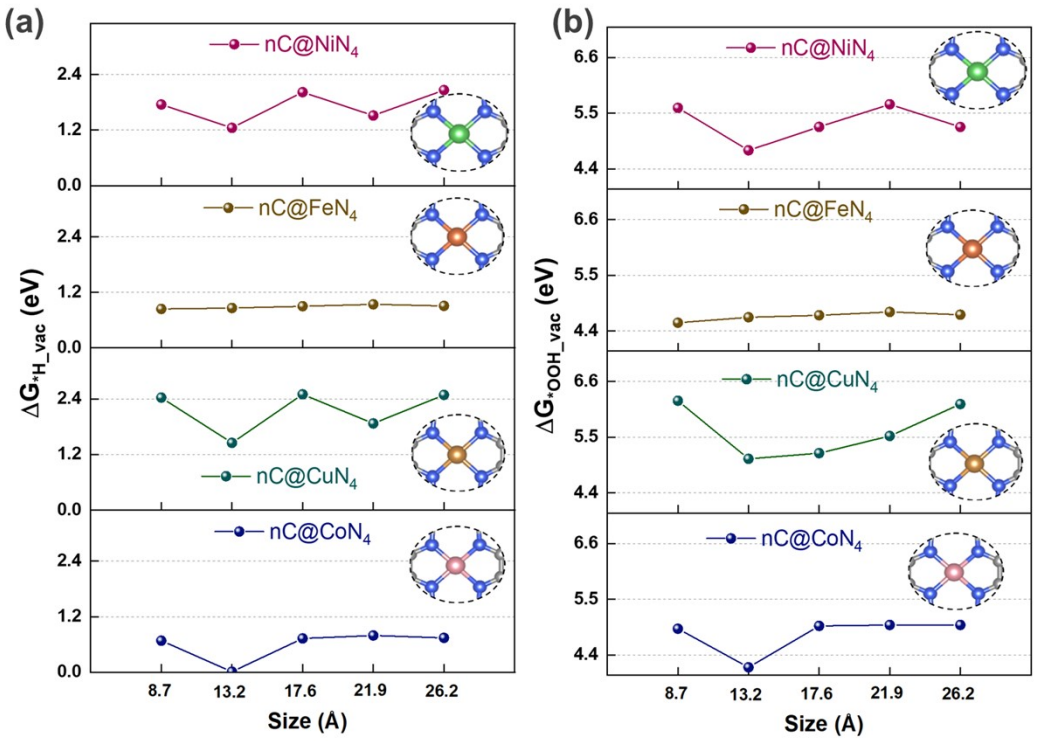

Figure S7. Size-dependent trends in nC@MN_4 (M = Ni, Fe, Cu, Co): (a) ΔG_{*H_vac} as a function of size; (b) ΔG_{*OOH_vac} as a function of size.

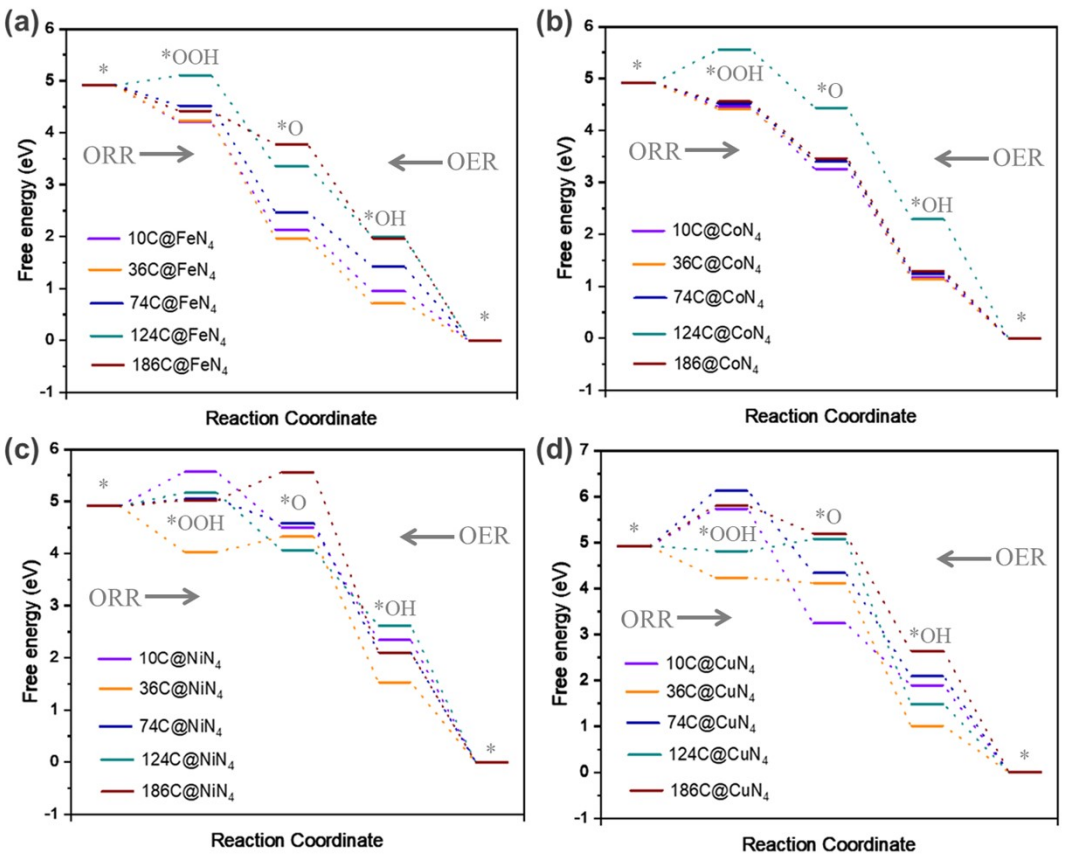

Figure S8. Free energy evolution diagrams for ORR/OER at different sizes of: (a)nC@FeN_4, (b)nC@CoN_4, (c)nC@NiN_4, (d)nC@CuN_4.

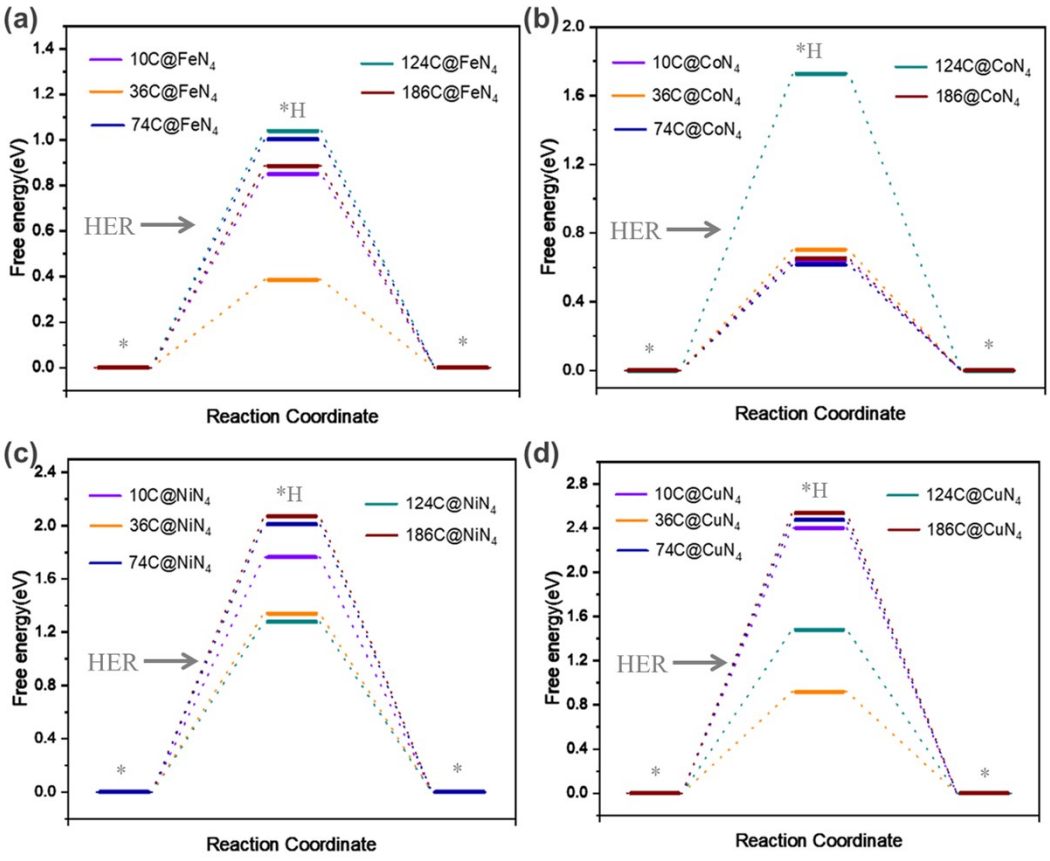

Figure S9. Free energy evolution diagrams for HER at different sizes of: (a)nC@FeN_4, (b)nC@CoN_4, (c)nC@NiN_4, (d)nC@CuN_4.

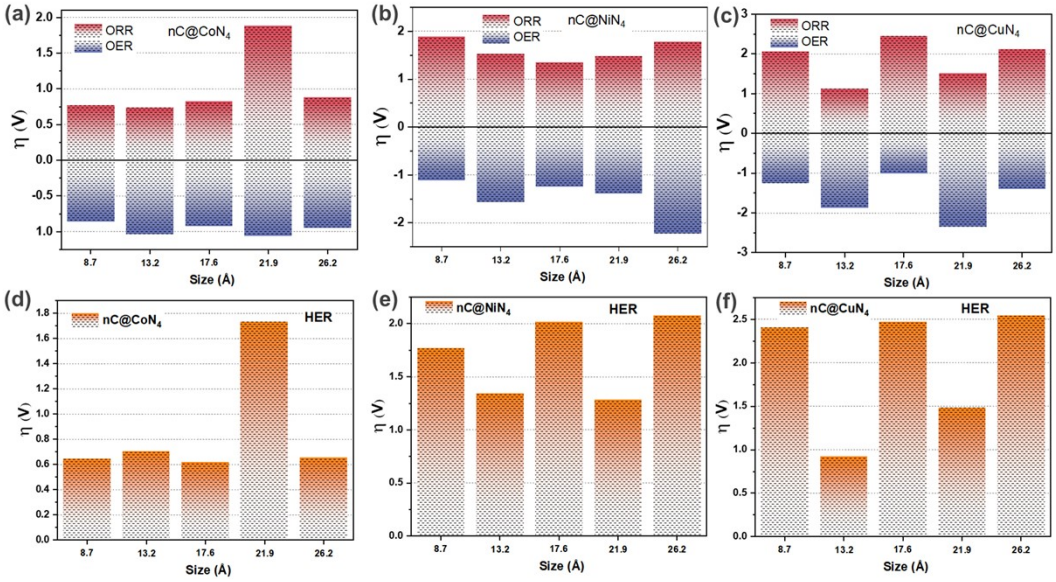

Figure S10. Overpotentials for different sizes of $nC@CoN_4$, $nC@NiN_4$, and $nC@CuN_4$: (a) ORR/OER overpotentials for $nC@CoN_4$; (b) ORR/OER overpotentials for $nC@NiN_4$; (c) ORR/OER overpotentials for $nC@CuN_4$; (d) HER overpotentials for $nC@CoN_4$; (e) HER overpotentials for $nC@NiN_4$; (f) HER overpotentials for $nC@CuN_4$.

References:

(1) Gaussian 09, Revision D.01, M. J. Frisch, G. W. Trucks, H. B. Schlegel, G. E. Scuseria, M. A. Robb, J. R. Cheeseman, G. Scalmani, V. Barone, B. Mennucci, G. A. Petersson, H. Nakatsuji, M. Caricato, X. Li, H. P. Hratchian, A. F. Izmaylov, J. Bloino, G. Zheng, J. L. Sonnenberg, M. Hada, M. Ehara, K. Toyota, R. Fukuda, J. Hasegawa, M. Ishida, T. Nakajima, Y. Honda, O. Kitao, H. Nakai, T. Vreven, J. A. Montgomery, Jr., J. E. Peralta, F. Ogliaro, M. Bearpark, J. J. Heyd, E. Brothers, K. N. Kudin, V. N. Staroverov, T. Keith, R. Kobayashi, J. Normand, K. Raghavachari, A. Rendell, J. C. Burant, S. S. Iyengar, J. Tomasi, M. Cossi, N. Rega, J. M. Millam, M. Klene, J. E. Knox, J. B. Cross, V. Bakken, C. Adamo, J. Jaramillo, R. Gomperts, R. E. Stratmann, O. Yazyev, A. J. Austin, R. Cammi, C. Pomelli, J. W. Ochterski, R. L. Martin, K. Morokuma, V. G. Zakrzewski, G. A. Voth, P. Salvador, J. J. Dannenberg, S. Dapprich, A. D. Daniels, O. Farkas, J. B. Foresman, J. V. Ortiz, J. Cioslowski, and D. J. Fox, Gaussian, Inc., Wallingford CT, 2013.

(2) Chai, J. Da; Head-Gordon, M. Long-Range Corrected Hybrid Density Functionals with Damped Atom-Atom Dispersion Corrections. *Physical Chemistry Chemical Physics* 2008, *10* (44), 6615–6620. https://doi.org/10.1039/b810189b.

(3) Weigend, F.; Ahlrichs, R. Balanced Basis Sets of Split Valence, Triple Zeta Valence and Quadruple Zeta Valence Quality for H to Rn: Design and Assessment of Accuracy. *Physical Chemistry Chemical Physics* 2005, *7* (18), 3297–3305. https://doi.org/10.1039/b508541a.

(4) Marenich, A. V.; Cramer, C. J.; Truhlar, D. G. Universal Solvation Model Based on Solute Electron Density and on a Continuum Model of the Solvent Defined by the Bulk Dielectric Constant and Atomic Surface Tensions. *Journal of Physical Chemistry B* 2009, *113* (18), 6378–6396. https://doi.org/10.1021/jp810292n.

(5) Xie, L.; Zhou, W.; Qu, Z.; Ding, Y.; Gao, J.; Sun, F.; Qin, Y. Understanding the Activity Origin of Oxygen-Doped Carbon Materials in Catalyzing the Two-Electron Oxygen Reduction Reaction towards Hydrogen Peroxide Generation. *J Colloid Interface Sci* 2022, *610*, 934–943. https://doi.org/10.1016/j.jcis.2021.11.144.

(6) Wang, Y.; Tang, Y. J.; Zhou, K. Self-Adjusting Activity Induced by Intrinsic Reaction Intermediate in Co-N-C Single-Atom Catalysts. *J Am Chem Soc* 2019, *141* (36), 14115–14119. https://doi.org/10.1021/jacs.9b07712.

(7) Lu, T.; Chen, F. Multiwfn: A Multifunctional Wavefunction Analyzer. *J Comput Chem* 2012, *33* (5), 580–592. https://doi.org/10.1002/jcc.22885.

(8) Lu, T.; Chen, F. Atomic Dipole Moment Corrected Hirshfeld Population Method. *J Theor Comput Chem* 2012, *11* (1), 163–183. https://doi.org/10.1142/S0219633612500113.

(9) Nørskov, J. K.; Abild-Pedersen, F.; Studt, F.; Bligaard, T. Density Functional Theory in Surface Chemistry and Catalysis. *Proceedings of the National Academy of Sciences of the United States of America*. January 18, 2011, pp 937–943. https://doi.org/10.1073/pnas.1006652108.

(10) Bhattacharjee, S.; Waghmare, U. V.; Lee, S. C. An Improved D-Band Model of the Catalytic Activity of Magnetic Transition Metal Surfaces. *Sci Rep* 2016, *6*. https://doi.org/10.1038/srep35916.

(11) Bredas, J. L. Mind the Gap! *Mater Horiz* 2014, *1* (1), 17–19. https://doi.org/10.1039/c3mh00098b.

(12) Zirzlmeier, J.; Schrettl, S.; Brauer, J. C.; Contal, E.; Vannay, L.; Brémond, É.; Jahnke, E.;

Guldi, D. M.; Corminboeuf, C.; Tykwinski, R. R.; Frauenrath, H. Optical Gap and Fundamental Gap of Oligoynes and Carbyne. *Nat Commun* 2020, *11* (1). https://doi.org/10.1038/s41467-020-18496-4.

(13) Nørskov, J. K.; Rossmeisl, J.; Logadottir, A.; Lindqvist, L.; Kitchin, J. R.; Bligaard, T.; Jónsson, H. Origin of the Overpotential for Oxygen Reduction at a Fuel-Cell Cathode. *Journal of Physical Chemistry B* 2004, *108* (46), 17886–17892. https://doi.org/10.1021/jp047349j.